ACCOUNTS of chemical research

Article

pubs.acs.org/accounts

An Expanded Palette of Xenon-129 NMR Biosensors

Yanfei Wang and Ivan J. Dmochowski*

Department of Chemistry, University of Pennsylvania, 231 South 34th Street, Philadelphia, Pennsylvania 19104, United States

CONSPECTUS: Molecular imaging holds considerable promise for elucidating biological processes in normal physiology as well as disease states, by determining the location and relative concentration of specific molecules of interest. Proton-based magnetic resonance imaging (^{1}H MRI) is nonionizing and provides good spatial resolution for clinical imaging but lacks sensitivity for imaging low-abundance (i.e., submicromolar) molecular markers of disease or environments with low proton densities. To address these limitations, hyperpolarized (hp) ^{129}Xe NMR spectroscopy and MRI have emerged as attractive complementary methodologies. Hyperpolarized xenon is nontoxic and can be readily delivered to patients via inhalation or injection, and improved xenon hyperpolarization technology makes it feasible to image the lungs and brain for clinical applications.

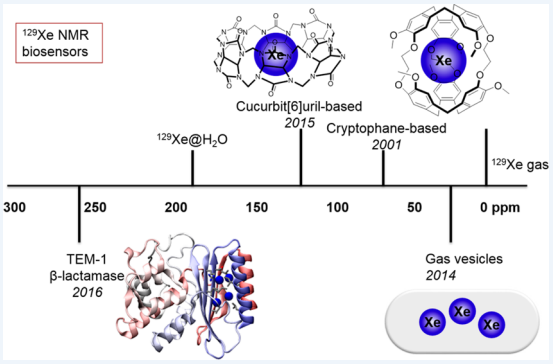

In order to target hp ^{129}Xe to biomolecular targets of interest, the concept of "xenon biosensing" was first proposed by a Berkeley team in 2001. The development of xenon biosensors has since focused on modifying organic host molecules (e.g., cryptophanes) via diverse conjugation chemistries and has brought about numerous sensing applications including the detection of peptides, proteins, oligonucleotides, metal ions, chemical modifications, and enzyme activity. Moreover, the large (~300 ppm) chemical shift window for hp ^{129}Xe bound to host molecules in water makes possible the simultaneous identification of multiple species in solution, that is, multiplexing. Beyond hyperpolarization, a 10^6-fold signal enhancement can be achieved through a technique known as hyperpolarized ^{129}Xe chemical exchange saturation transfer (hyper-CEST), which shows great potential to meet the sensitivity requirement in many applications.

This Account highlights an expanded palette of hyper-CEST biosensors, which now includes cryptophane and cucurbit[6]uril (CB[6]) small-molecule hosts, as well as genetically encoded gas vesicles and single proteins. In 2015, we reported picomolar detection of commercially available CB[6] via hyper-CEST. Inspired by the versatile host−guest chemistry of CB[6], our lab and others developed "turn-on" strategies for CB[6]-hyper-CEST biosensing, demonstrating detection of protein analytes in complex media and specific chemical events. CB[6] is starting to be employed for *in vivo* imaging applications. We also recently determined that TEM-1 β-lactamase can function as a single-protein reporter for hyper-CEST and observed useful saturation contrast for β-lactamase expressed in bacterial and mammalian cells. These newly developed small-molecule and genetically encoded xenon biosensors offer significant potential to extend the scope of hp ^{129}Xe toward molecular MRI.

1. INTRODUCTION

Magnetic resonance imaging (MRI) is a well-established clinical imaging method with good spatial resolution and excellent tissue penetration ability. Pioneering work in the development of ^{1}H MRI contrast agents has enabled stimuli-responsive detection of metabolites including enzymes, signaling molecules, and pH values of local environments, but such agents do not allow detection of most analytes at physiologic concentration.[1] Paramagnetic contrast agents function by affecting thermally polarized ^{1}H nuclei in the local environment; therefore, high micromolar (or greater) concentrations of contrast agent are typically needed.

Hyperpolarized (hp) ^{129}Xe NMR and MRI have emerged as attractive complements to ^{1}H MRI and have been investigated in many applications that require significant enhancements in detection sensitivity.[2−5] The isotope ^{129}Xe is spin-1/2 and possesses several favorable physical properties that make it a unique candidate for molecular imaging. First, xenon is very soluble in organic solvents such as hexane and benzene, as well as aqueous solutions including blood plasma. As a result, xenon will partition between different solvents or between blood and tissue, and this feature can be utilized for certain imaging applications. Second, the large and highly polarizable electron cloud of xenon affords high affinity for void spaces as well as sensitivity to its local environment. This translates to a large (~300 ppm) chemical shift window for ^{129}Xe bound to different organic host molecules in aqueous solution.[6] Consequently, xenon can display well-resolved chemical shifts, corresponding to the solvent, small molecules, or proteins with which it associates. Third, ^{129}Xe can be hyperpolarized (hp) through a two-step process called spin exchange optical pumping where polarization is transferred from electronically polarized Rb atoms in the vapor state to ^{129}Xe nuclei.[7] The ^{129}Xe NMR signal can be increased by more than 10000-fold upon hyperpolarization. Therefore, low (i.e., micromolar)

Received: June 22, 2016
Published: September 19, 2016

DOI: 10.1021/acs.accounts.6b00309
Acc. Chem. Res. 2016, 49, 2179−2187

concentrations of hp ^{129}Xe can produce intense NMR signals. Xenon is found in trace quantities in air; thus there is no background signal competing with exogenously supplied hp ^{129}Xe.

Finally, for the purpose of *in vivo* imaging, hp ^{129}Xe has lower toxicity compared to most paramagnetic metals currently used as contrast agents for proton-based MRI. The long T_1 of hp ^{129}Xe in both gas phase (with the longest measured T_1 of 99 h at 14.1 T[8]) and dissolved phase (~66 s in saline water at 9.4 T[9]) helps in sustaining the hp ^{129}Xe signal during transport from the hyperpolarizer to the detection region. It is also worth noting that because signal averaging in hp MRI is not based on relaxation recovery but on renewed delivery of hp species for each scan, long T_1 does not slow image acquisition. These favorable properties of xenon have led to many *in vivo* imaging studies. Albert et al. first used xenon to image a mouse lung;[10] subsequently, there have been many examples of ^{129}Xe-based imaging of human lungs, chest, and brain,[11] which confirm the biocompatibility of xenon-based MRI.

2. CRYPTOPHANE-BASED XENON BIOSENSORS

2.1. Cryptophane Characterization

It was discovered in 1998 that cryptophane-A binds xenon reversibly and with good affinity ($K_A \approx 3000$ M^{-1} at rt in $C_2D_2Cl_4$), and the xenon exchange rate is sufficiently slow to give well separated xenon signals on a NMR spectrum.[12,13] Early work on cryptophane synthesis and studies of xenon complexation was reviewed extensively by Brotin and Dutasta.[14] In 2011, we reported a shorter six-step synthesis of trifunctionalized cryptophane-A derivatives with an improved yield of 6%,[15] building on the work of Brotin et al., who reported a milder $Sc(OTf)_3$ cyclization for cyclotriguiacylene formation.[16] The use of either tripropargyl cryptophane with azide−alkyne cycloaddition(s) or trihydroxy cryptophane with ether linkage(s) allows functionalization of cryptophane with solubilizing or targeting moieties. Our trifunctionalized water-soluble cryptophanes, triacetic acid cryptophane (TAAC),[17] tris(triazole propionic acid) cryptophane (TTPC),[18] and tris(triazole ethylamine) cryptophane (TTEC),[19] showed similar water solubility to the reported hexa-functionalized cryptophanes[20] but exhibited significantly higher xenon-binding affinities. To rationalize these differences, molecular simulation and free energy perturbation methods were applied to estimate the affinities of Xe for TAAC, TTPC, and TTEC, as well as three hexa-acid water-soluble cryptophanes with varying cavity size.[21] The simulations showed that displacement of water from the host cavity is a key component of the xenon binding equilibrium, and the average number of water molecules within the cavity is strongly anticorrelated with the free energy of Xe binding to the different cryptophanes.[21]

We also investigated host−guest interactions in cryptophanes by X-ray crystallography. Co-crystallization of cryptophane-A derivatives with methanol, xenon, and chloroform revealed that the cavity internal volume (80−102 Å^3) varied with guest size.[22] Importantly, we observed that in the xenon-bound structure, van der Waals interactions were nearly optimized, with intermediate interior cavity volume of 85−89 Å^3 and guest/host volume ratio of 0.47−0.49. This ratio was found previously to reside ideally near 0.55 for host−guest interactions relying purely on dispersion interactions.[23]

2.2. Biosensors

Xenon biosensing can be achieved by conjugating specific targeting and water-solubilizing group(s) to cryptophane. The xenon biosensor usually functions by producing a different ^{129}Xe NMR chemical shift when bound to the target, due to the sensitivity of the xenon nuclear spin to any perturbation of the large electron cloud. The first xenon biosensor, developed by Pines and co-workers in 2001, covalently modified cryptophane-A with a peptide as the solubilizing element and biotin as the targeting element.[24] A measurable shift, ~2.3 ppm, was observed for the xenon biosensor bound to avidin. In a follow-up study, one resonance was observed for monoallyl-substituted cryptophane-A, and upon conjugation of the chiral peptide, two peaks 0.15 ppm apart appeared,[25] which were attributed to the diastereomers. The observed sensitivity of xenon to diastereomerism is problematic for many biosensing applications, because it dilutes the xenon-biomarker signal and complicates peak assignments as well as efforts to selectively irradiate ^{129}Xe in a specific environment, as required for many NMR experiments.

In 2006, our laboratory demonstrated the ability of hp ^{129}Xe to report on protease activity by appending cryptophane with a peptide substrate for matrix metalloproteinase-7, a known cancer biomarker.[26] In a next study, researchers utilized enantiopure cryptophane-A grafted to a 20-mer oligonucleotide to detect DNA binding.[27] The ^{129}Xe NMR peak for biosensor plus complementary DNA strand was shifted 1.5 ppm upfield, with only one bound peak as expected for single enantiomers. However, at increasing concentration, both biosensor alone and biosensor plus noncomplementary strand exhibited multiple Xe@biosensor peaks. This was hypothesized to be a result of microemulsions and micelles or vesicles formed at higher concentration.[27] This observation highlights the importance of well-solubilized xenon biosensors. Most recently, Kotera et al. attached hexa-carboxylate cryptophane to two arsenic moieties capable of interacting with proteins that contain a tetracysteine tag and observed a single peak that was shifted 6.4 ppm upon addition of excess Cys4-tagged peptide.[28]

We also developed xenon biosensors targeting integrin receptors that are upregulated in many human cancers. Cryptophane was functionalized with a single linear $(RGD)_4$ peptide repeat[29] or with a cyclic RGDyK peptide and two 3-azidopropionic acids.[30] We observed only one 4.1 ppm downfield-shifted peak when the biosensor bound to $\alpha_v\beta_3$ integrin, indicating again that with a well-solubilized cryptophane it was possible to engage protein targets using short tethers and obtain well-resolved ^{129}Xe NMR spectra. In order to investigate the cell compatibility of xenon biosensors, we fluorescently labeled the cRGDyK-cryptophane and performed cell uptake, viability, and specificity studies.[30] This work demonstrated targeting of $\alpha_v\beta_3$ integrin and $\alpha_{IIb}\beta_3$ integrin with nanomolar affinity and specificity and low cytotoxicity at concentrations required for NMR experiments, which paved the way for cellular hp ^{129}Xe NMR spectroscopy and imaging experiments.[31−33]

We have used carbonic anhydrase II (CAII) and CAI, cytosolic isoforms of α-CA, as the archetype to guide the development of xenon biosensors.[34−36] The unique ^{129}Xe NMR chemical shifts for biosensors bound to CAI or CAII demonstrate the potential of xenon biosensors to discriminate between isoforms of α-CA, including the cancer biomarkers CAIX and CAXII.

DOI: 10.1021/acs.accounts.6b00309
Acc. Chem. Res. 2016, 49, 2179−2187

2.3. Enhanced Detection

The hyperpolarization of xenon makes it possible to detect directly the signals from low concentrations of biosensors. When the concentration of biosensor is low compared to dissolved xenon, the dissolved xenon can act as a polarization reservoir if just the magnetization of caged xenon is excited during signal acquisition. This can be achieved by applying selective pulses when the resonances are well separated.[37] With a 0.1−0.15 s delay between excitation pulses, there is effectively full recovery of the caged xenon magnetization, and hence many acquisitions can be taken before the dissolved hp xenon pool is exhausted. This soft-pulse approach relies on signal averaging based on the exchange of xenon and allows for detection of low-micromolar cryptophane.

Detection sensitivity can be further improved via the hyper-CEST technique, which relies on the initial hp ^{129}Xe signal, as well as modulation by chemical exchange saturation transfer (CEST). Specifically, the ^{129}Xe@host spin pool is saturated by frequency-selective RF pulses, and through chemical exchange, the saturated spins transfer to the bulk xenon spin pool where loss of signal is monitored.[38] Selective RF pulses are applied for a long period compared to the mean xenon residence time inside cryptophane-A (~1 ms at 320 K), allowing for a single cryptophane molecule to saturate thousands of xenon spins by the simplest mechanism (Scheme 1). This method improved the detection sensitivity of water-soluble cryptophane to the nanomolar and picomolar range, without the need for long acquisition times.[38,39] A similar *in vivo* MRI approach, xenon transfer contrast (XTC), initially took advantage of the exchange between xenon in gas phase and that in solution phase to probe lung physiology.[40]

Scheme 1. Chemical Structures of CB[6] and TAAC (Top) and Hyper-CEST Mechanism Involving Xenon-Binding Molecules Represented by Hexagons (Bottom)

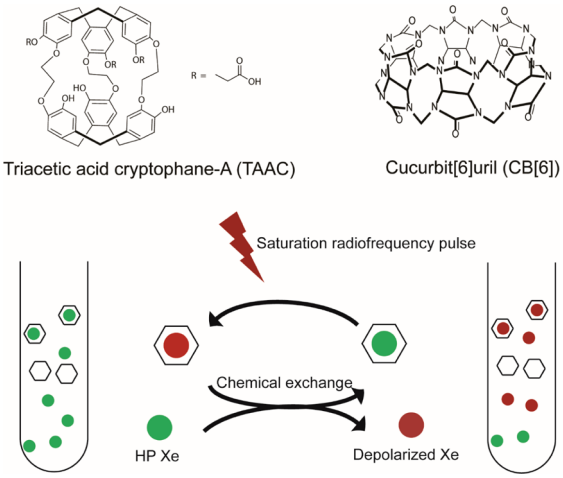

Reproduced with permission from ref 55. Copyright 2015 Royal Society of Chemistry.

Since its development in 2006, hyper-CEST has been applied in many biosensing applications. In 2009, Schlundt et al.[41] modified cryptophane with a hemagglutinin peptide, which binds to a major histocompatibility complex protein, and observed a 1-ppm downfield shift. More recently, Schröder and co-workers acquired hyper-CEST MR images of cell-internalized fluorescein-bearing cryptophane conjugates,[31] of a peptide-functionalized liposomal carrier targeting brain endothelial cells,[42] metabolically labeled cell-surface glycans,[43] and cells targeted by antibody-based modular biosensors.[44]

Our laboratory recently developed a ^{129}Xe biosensor that labels cancer cells at acidic pH.[45] The cryptophane biosensor was attached to a 30mer EALA-repeat peptide that is α-helical at pH 5.5 and disordered at pH 7.5. The ^{129}Xe NMR chemical shift at rt was strongly pH-dependent ($\Delta\delta$ = 3.4 ppm): δ = 64.2 ppm at pH 7.5 vs δ = 67.6 ppm at pH 5.5. Using hyper-CEST, peptido-cryptophane was detected at low-picomolar (10^{-11} M) concentration. As designed, in biosensor-HeLa cell solutions, peptide-cell membrane insertion at pH 5.5 generated a 13.4 ppm downfield cryptophane-^{129}Xe NMR chemical shift relative to pH 7.5 studies (Figure 1). The larger separation of the two resonances was induced by the insertion of cryptophane into lipid membrane, as observed in other studies.[31−33]

2.4. Continued Optimization of Xe Biosensors

The modular construction of xenon biosensors allows chemical linkage of the host molecule to a wide range of targeting agents. A moderate length linker affords flexibility and holds cryptophane and binding moiety in proximity, which generates narrow ^{129}Xe NMR lines while retaining the chemical shift response to the binding event.[35,46]

To increase sensitivity, multiple cryptophanes have been tethered to each targeting element, thereby increasing local concentration of xenon. This concept was first demonstrated by Mynar et al., who observed moderate ^{129}Xe signal enhancement using multiple cryptophanes in a dendrimer with one targeting attachment.[47] Higher sensitivity was later achieved by covalently attaching several cryptophanes to one targeting module through avidin−biotin bridges[44] or many cryptophanes to spherical or rod-like viral capsids.[32,48,49] The dual signal amplification from multiple cryptophanes per target and many xenon atoms per cryptophane via hyper-CEST greatly expanded the potential of using xenon biosensors for localized and sensitive target detection.

3. HYPERPOLARIZED XENON IN BIOMATERIALS

Hyperpolarized xenon has also been used alone to characterize biological environments. Initially, Albert et al. showed that xenon in the presence of red blood cells gave rise to two signals in the NMR spectrum.[50] The ~20 ppm separation between two peaks was attributed to the interaction of xenon with hemoglobin present in the intracellular compartment of RBCs.[9] In 2011, Berthault and co-workers reported the ^{129}Xe NMR spectra of prokaryotic, eukaryotic, vegetal, and yeast cells, where two signals separated by only a few ppm at high cell density (10^7−10^8 mammalian cells/mL) were observed.[51]

In 2014, our laboratory employed hyper-CEST to detect *Bacillus anthracis* and *Bacillus subtilis* spores in solution and interrogate the layers that comprise their structures.[52] Removal of the outermost spore layers in *B. anthracis* and *B. subtilis* (the exosporium and coat, respectively) enhanced ^{129}Xe exchange with the spore interior and therefore increased the hyper-CEST saturation contrast. The most Xe-accessible spore sample (strain AD142) was detected at a concentration below 1 fM. Notably, the spores were invisible by hp ^{129}Xe NMR direct detection methods, highlighting the lack of high-affinity xenon-binding sites, and the potential for extending hyper-CEST NMR analysis to other biological and synthetic nanoporous structures.

DOI: 10.1021/acs.accounts.6b00309
Acc. Chem. Res. 2016, 49, 2179−2187

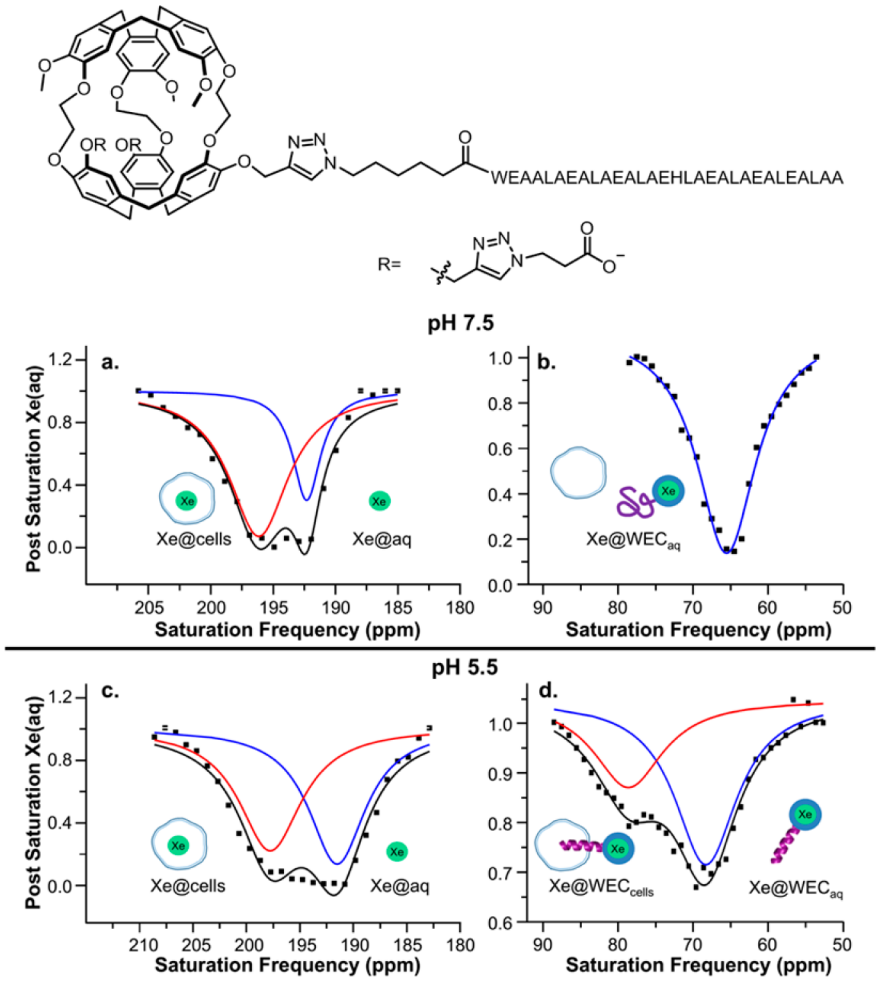

Figure 1. (top) Chemical structure of water-soluble EALA-cryptophane (WEC). (bottom) Hyper-CEST ^{129}Xe NMR spectra for 5−10 μM WEC in a suspension of 1 × 10^7 cells/mL at pH 7.5: (a) Xe@cells, red trace; Xe@aq, blue trace; (b) Xe@WEC$_{aq}$ and at pH 5.5; (c) Xe@cells, red trace; Xe@aq, blue trace; (d) Xe@WEC$_{cells}$, red trace; Xe@WEC$_{aq}$, blue trace. Reproduced with permission from ref 45. Copyright 2015 American Chemical Society.

4. CUCURBIT[6]URIL BASED XENON-129 NMR BIOSENSORS

Cryptophane-based xenon biosensors require multistep synthesis and are isolated in low yield. New xenon-binding contrast agents have recently expanded applications of hp ^{129}Xe in chemical sensing and imaging. Stevens et al. reported a perfluorocarbon nanoemulsion contrast agent for ^{129}Xe NMR, with each droplet encapsulating multiple xenon atoms.[53] Nanoemulsions with droplet diameters between 160 and 310 nm were detected at concentrations as low as 100 fM, using hyper-CEST. Perfluorocarbon nanodroplets were later shown to be internalized by cells and detected sensitively.[54]

Our laboratory found that commercially available cucurbit[6]uril (CB[6]) with a cavity that is hydrophobic, rigidly open, and of similar dimensions to Xe (diameter ∼4.3 Å), can promote rapid Xe exchange interactions, as required for hyper-CEST.[55] The hp ^{129}Xe NMR spectrum obtained with 5 mM CB[6] using a direct detection method showed that the ^{129}Xe−CB[6] peak in pH 7.2 PBS was 72 ppm upfield-shifted from the ^{129}Xe-water peak. Xe affinity determined for CB[6] in PBS at 300 K was ∼40-fold lower than that measured previously for TAAC.[18] However, the ^{129}Xe−CB[6] exchange rate was ∼17-fold higher than previously measured for ^{129}Xe−TAAC (k_{exch} = 86 s^{-1}) at 300 K.[39] Ultrasensitive (1.8 pM) detection of CB[6] via hyper-CEST was achieved by applying shaped RF saturation pulses at the chemical shift of ^{129}Xe in CB[6] and measuring the residual aqueous ^{129}Xe signal after spin transfer as on-resonance CEST response.

We sought to exploit the versatile host−guest chemistry of CB[6] to develop a *de novo* "molecular relay" that reports on specific proteins in solution.[56] CB[6]-based ^{129}Xe NMR biosensors were programmed for three sequential recognition events: a two-faced guest (TFG) initially binds CB[6], the TFG is sequestered by cognate protein thereby freeing CB[6], and last, xenon binds CB[6] for ultrasensitive detection by hyper-CEST. The TFG is engineered to control this relay, such that CB[6]−^{129}Xe NMR signal is absent until addition of analyte. In our initial study, we designed TFGs with a CAII-binding *p*-benzenesulfonamide moiety and CB[6]-binding butylamine tail, while varying the length and chemical structure of the linker. Upon addition of excess TFG to CB[6], the ^{129}Xe−CB[6] signal was greatly reduced as a result of less free CB[6] in solution. Upon CAII addition, ^{129}Xe−CB[6] hyper-CEST signal was mostly restored, confirming that TFG was sequestered by CAII. Cell studies highlighted the ability of the CB[6] detection scheme to identify a specific protein target within a complex mixture (Figure 2).

DOI: 10.1021/acs.accounts.6b00309
Acc. Chem. Res. 2016, 49, 2179−2187

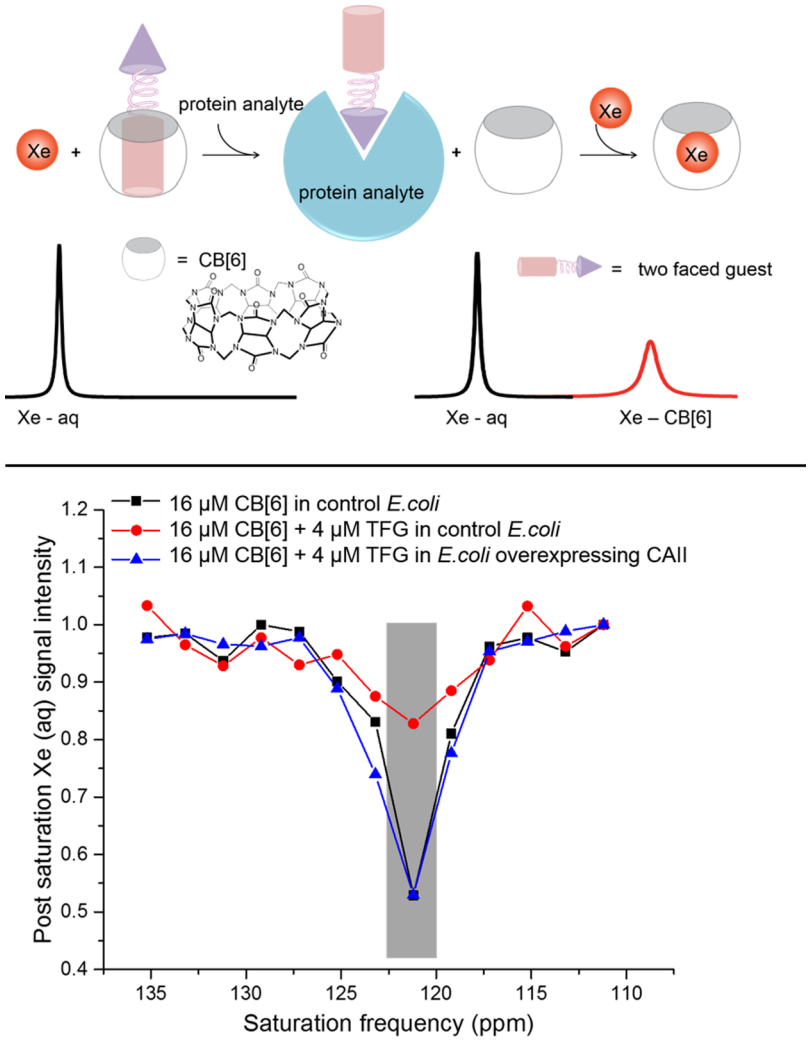

Figure 2. (top) Molecular relay producing ^{129}Xe NMR signal upon analyte detection. (bottom) Frequency-dependent hyper-CEST spectra showed CAII detection via CB[6] relay in bacterial lysate (OD_{600nm} = 2) at 300 K. Reproduced with permission from ref 56. Copyright 2015 Wiley–VCH.

CB[6] has gained attention for its excellent hyper-CEST response, comparable to previously used cryptophane constructs.[57] For example, in 2015, Schröder et al. reported an enzyme-sensing platform based on a competition between ^{129}Xe and an enzyme product for binding to the CB[6] cavity.[58] And, the Pines group designed a CB[6]–rotaxane platform where a cyclodextrin stopper prevents ^{129}Xe from accessing the CB[6] cavity until a specific cleavage event releases CB[6] to produce a ^{129}Xe@CB[6] signal.[59] Most recently, magnetic resonance images and a hyper-CEST saturation map of CB[6] in whole bovine blood were reported.[60]

Cryptophane-based xenon biosensing strategies have mostly relied on small chemical shift differences between target-bound and unbound states, which requires high spectral resolution that can be challenging in hyper-CEST mode. Thus, the turn-on strategies reported with CB[6] offer advantages by suppressing the ^{129}Xe@host signal until the sensor reaches a region of interest or is selectively activated.

5. GENETICALLY-ENCODED PROTEIN AS A ^{129}Xe NMR REPORTER

There has been long-standing interest in developing genetically encoded MRI reporters that combine high-resolution, non-invasive MRI with the power of molecular biology to visualize specific molecular processes. However, previous efforts to develop such reporters for ^{1}H MRI have been limited by low detection sensitivity.[61] This has motivated investigation of hyper-CEST contrast agents, which can provide Xe-specific molecular details in the context of an anatomical ^{1}H MR image. In 2014, Shapiro et al. reported the use of genetically encoded bacterial gas vesicles (GVs) as ultrasensitive hyper-CEST contrast agents, detectable at picomolar concentration.[62] This pioneering example of a hyper-CEST reporter gene is translationally challenging because GVs are very large (0.1–2 μm long) multimeric protein assemblies from complex gene clusters and difficult to reconstitute in many eukaryotic systems.

Our lab has endeavored to develop a genetically encoded single protein as a hyper-CEST reporter.[63] We initially considered TEM-1 β-lactamase (bla) based on its well-established allosteric site whose size and hydrophobicity suggest it to be a good target for Xe exchange. We observed two saturation responses in the hyper-CEST z-spectrum for 80 μM bla: one free ^{129}Xe in solution peak centered at 195 ppm, and a second peak centered at 255 ppm that results from ^{129}Xe–bla interaction. Importantly, the unique ^{129}Xe–bla peak cannot be directly observed by hp ^{129}Xe NMR spectroscopy even with high-concentration (approximately millimolar) bla, due to the low xenon-bound population and high rate of xenon

DOI: 10.1021/acs.accounts.6b00309
Acc. Chem. Res. 2016, 49, 2179–2187

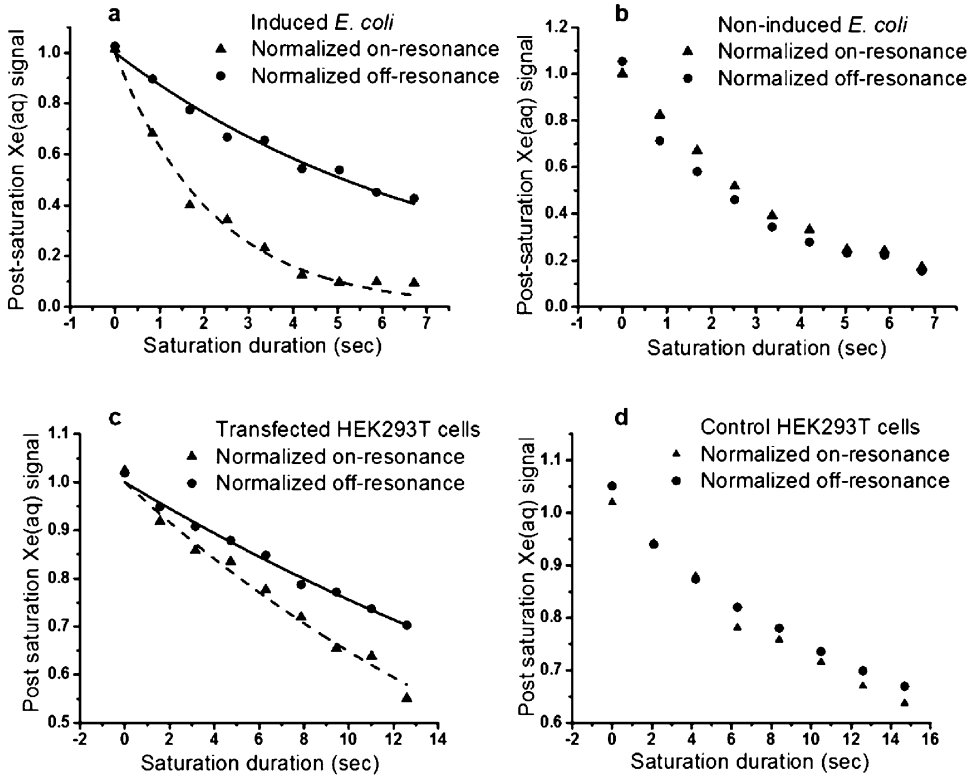

Figure 3. (top) Time-dependent saturation transfer data for induced *E. coli* (a) and noninduced *E. coli* (b). (bottom) Time-dependent saturation transfer data for transfected (c) and control (d) HEK293T/17 cells. Reproduced with permission from ref 63. Copyright 2016 Wiley−VCH.

exchange between different sites. We carried out hyper-CEST measurements by varying saturation time to determine the molecular sensitivity of bla and showed that 0.1 μM (2.9 μg/mL) bla was able to produce 23% ± 2% saturation contrast. The *in vitro* detection limit of single protein bla is comparable to previously reported GVs in terms of protein mass concentration[62] and represents a roughly 100-fold improvement compared to ^{1}H-CEST reporter genes.[64]

We then investigated the possibility of using bla as a genetically encoded ^{129}Xe NMR reporter. BL21(DE3) *E. coli* cells expressing recombinant wt-bla were induced with isopropyl-β-thiogalactopyranoside, and hyper-CEST experiments showed a saturation contrast of 72% ± 3% for cells at OD_{600} of 9.2. By contrast, the on-resonance and off-resonance curves were almost identical for the control *E. coli* sample at the same OD_{600}. We also tested whether bla can function in mammalian cells and found that 0.2 million/mL transfected HEK cells producing the equivalent of 0.7 μM bla in the cell suspension was sufficient to produce a saturation contrast of 13% ± 1%, compared to minimal contrast observed for control HEK cells (Figure 3).

This study highlights a potential use for hp ^{129}Xe as an ultrasensitive probe for studying allosteric pockets in proteins. Moreover, bla has been well established as a fluorogenic reporter for *in vivo* studies, which lends support to its development as a hyper-CEST reporter for biomolecular imaging. Bla mutagenesis should make it possible to increase Xe affinity at the primary site and also shift the hyper-CEST response peak, either to achieve multiplexing or to discriminate against ^{129}Xe-mammalian cell background signals.

6. SUMMARY AND OUTLOOK

Further enhancement of detection sensitivity will be important in future applications but is somewhat context dependent. For example, in the hyper-CEST scheme, higher Xe exchange rates confer faster saturation transfer but also require more power for complete saturation and therefore reduce selectivity. The parameters for continuous-wave (CW) saturation were recently reported.[65] Moreover, to achieve optimal sensitivity, saturation of the encapsulated xenon should not perturb the bulk xenon pool, to ensure that biosensor-mediated saturation can be discerned from the natural relaxation processes. While saturation-transfer effects can be quantitatively predicted from the Bloch equations,[66] specific information that is not always known in advance is required, such as the inhomogeneous contribution to line width. The sensitivity also depends on the initial ^{129}Xe polarization level, rate and fluctuation of hp ^{129}Xe delivery, and relaxation rate of hp ^{129}Xe in the specific environment.

Translating *in vitro* experiments to *in vivo* imaging requires addressing additional issues such as delivery of hp Xe and biosensors to local sites of interest, and RF tissue heating during imaging. Previous study on the pharmacokinetics of hp Xe estimated that the maximum concentration of Xe that can be breathed is 80%,[67] and delivery of hp Xe through inhalation has enabled pulmonary and cerebral MRI in both animals and humans.[68] Hyperpolarized ^{129}Xe can be delivered into the bloodstream by injection of hp ^{129}Xe dissolved in physiological solution. For hp ^{129}Xe MR biosensing, the biosensors are administered to the organism before the delivery of hp ^{129}Xe. More work is needed to determine the biocompatibility and biodistribution of CB[6], cryptophane, and other xenon-binding biosensors. Promising structures are zeolite nano-

DOI: 10.1021/acs.accounts.6b00309
Acc. Chem. Res. 2016, 49, 2179−2187

particles, for which the localization and biodistribution have been studied after injection into mice.[69] The high sensitivity of hyper-CEST experiments depends on highly efficient saturation but is constrained by limits on specific absorption rate (SAR) of the pulses for *in vivo* studies. It has been shown that, compared with CW saturation, pulsed saturation can achieve comparable saturation efficiency at lower power, thus minimizing RF heating.[70] Recently, hyper-CEST data with CB[6] in whole blood was reported using prepulse train with a SAR of 0.025 W/kg, well below the FDA limit of 4 W/kg.[60]

Importantly, ^{129}Xe contrast agents should be amenable to multiplexed detection, due to the large ^{129}Xe NMR chemical shift window for xenon bound to different biosensors.[54] The ability to visualize several biomarkers simultaneously will be particularly useful for disease diagnosis. Coupling hyper-CEST with multiplexing will require additional optimization to maximize molecular and spatial selectivity in different compartments. The continued development of better hp xenon delivery methods and more targeted, small-molecule and genetically encoded biosensors will help to expand the scope of hp ^{129}Xe MRI for molecular imaging.

AUTHOR INFORMATION

Corresponding Author

*E-mail: ivandmo@sas.upenn.edu.

Funding

This work was supported by Grant NIH R01-GM097478 and CDMRP-LCRP Concept Award No. LC130824.

Notes

The authors declare no competing financial interest.

Biographies

Yanfei Wang received her B.S. in chemistry from University of Science and Technology of China in 2011. In 2016, she completed Ph.D. studies at University of Pennsylvania under the supervision of Professor Ivan J. Dmochowski.

Ivan J. Dmochowski received B.A. in chemistry from Harvard College in 1994 and Ph.D. in chemistry from California Institute of Technology in 2000, where he trained with Harry Gray. He performed postdoctoral training with Scott Fraser at Caltech and, in 2003, joined the faculty at the University of Pennsylvania, where he is currently Professor and Undergraduate Chair of Chemistry.

REFERENCES

(1) Shapiro, M. G.; Atanasijevic, T.; Faas, H.; Westmeyer, G. G.; Jasanoff, A. Dynamic imaging with MRI contrast agents: quantitative considerations. *Magn. Reson. Imaging* **2006**, *24*, 449−462.

(2) Berthault, P.; Huber, G.; Desvaux, H. Biosensing using laser-polarized xenon NMR/MRI. *Prog. Nucl. Magn. Reson. Spectrosc.* **2009**, *55*, 35−60.

(3) Taratula, O.; Dmochowski, I. J. Functionalized ^{129}Xe contrast agents for magnetic resonance imaging. *Curr. Opin. Chem. Biol.* **2010**, *14*, 97−104.

(4) Palaniappan, K. K.; Francis, M. B.; Pines, A.; Wemmer, D. E. Molecular sensing using hyperpolarized xenon NMR spectroscopy. *Isr. J. Chem.* **2014**, *54*, 104−112.

(5) Schröder, L. Xenon for NMR biosensing − Inert but alert. *Phys. Medica* **2013**, *29*, 3−16.

(6) Miller, K. W.; Reo, N. V.; Schoot Uiterkamp, A. J.; Stengle, D. P.; Stengle, T. R.; Williamson, K. L. Xenon NMR: chemical shifts of a general anesthetic in common solvents, proteins, and membranes. *Proc. Natl. Acad. Sci. U. S. A.* **1981**, *78*, 4946−4949.

(7) Walker, T. G.; Happer, W. Spin-exchange optical pumping of noble-gas nuclei. *Rev. Mod. Phys.* **1997**, *69*, 629−642.

(8) Anger, B. C.; Schrank, G.; Schoeck, A.; Butler, K. A.; Solum, M. S.; Pugmire, R. J.; Saam, B. Gas-phase spin relaxation of (129)Xe. *Phys. Rev. A: At., Mol., Opt. Phys.* **2008**, *78*, 043406.

(9) Bifone, A.; Song, Y.-Q.; Seydoux, R.; Taylor, R. E.; Goodson, B. M.; Pietrass, T.; Budinger, T. F.; Navon, G.; Pines, A. NMR of laser-polarized xenon in human blood. *Proc. Natl. Acad. Sci. U. S. A.* **1996**, *93*, 12932−12936.

(10) Albert, M. S.; Cates, G. D.; Driehuys, B.; Happer, W.; Saam, B.; Springer, C. S., Jr.; Wishnia, A. Biological magnetic resonance imaging using laser-polarized ^{129}Xe. *Nature* **1994**, *370*, 199−201.

(11) Rao, M.; Stewart, N. J.; Norquay, G.; Griffiths, P. D.; Wild, J. M. High resolution spectroscopy and chemical shift imaging of hyper-polarized ^{129}Xe dissolved in the human brain in vivo at 1.5 T. *Magn. Reson. Med.* **2016**, *75*, 2227−2234.

(12) Gabard, J.; Collet, A. Synthesis of a(D3)-bis-(cyclotriveratrylenyl) macrocage by stereospecific replication of a(C3)-subunit. *J. Chem. Soc., Chem. Commun.* **1981**, 1137−1139.

(13) Bartik, K.; Luhmer, M.; Dutasta, J. P.; Collet, A.; Reisse, J. Xe-129 and H-1 NMR study of the reversible trapping of xenon by cryptophane-A in organic solution. *J. Am. Chem. Soc.* **1998**, *120*, 784−791.

(14) Brotin, T.; Dutasta, J.-P. Cryptophanes and their complexes-present and future. *Chem. Rev.* **2009**, *109*, 88−130.

(15) Taratula, O.; Hill, P. A.; Bai, Y.; Khan, N. S.; Dmochowski, I. J. Shorter synthesis of trifunctionalized cryptophane-A derivatives. *Org. Lett.* **2011**, *13*, 1414−1417.

(16) Brotin, T.; Roy, V.; Dutasta, J. P. Improved synthesis of functional CTVs and cryptophanes using $Sc(OTf)_3$ as catalyst. *J. Org. Chem.* **2005**, *70*, 6187−6195.

(17) Hill, P. A.; Wei, Q.; Troxler, T.; Dmochowski, I. J. Substituent effects on xenon binding affinity and solution behavior of water-soluble cryptophanes. *J. Am. Chem. Soc.* **2009**, *131*, 3069−3077.

(18) Hill, P. A.; Wei, Q.; Eckenhoff, R. G.; Dmochowski, I. J. Thermodynamics of xenon binding to cryptophane in water and human plasma. *J. Am. Chem. Soc.* **2007**, *129*, 11662−11662.

(19) Jacobson, D. R.; Khan, N. S.; Collé, R.; Fitzgerald, R.; Laureano-Pérez, L.; Bai, Y.; Dmochowski, I. J. Measurement of radon and xenon binding to a cryptophane molecular host. *Proc. Natl. Acad. Sci. U. S. A.* **2011**, *108*, 10969−10973.

(20) Huber, G.; Brotin, T.; Dubois, L.; Desvaux, H.; Dutasta, J. P.; Berthault, P. Water soluble cryptophanes showing unprecedented affinity for xenon: Candidates as NMR-based biosensors. *J. Am. Chem. Soc.* **2006**, *128*, 6239−6246.

(21) Gao, L.; Liu, W. H.; Lee, O. S.; Dmochowski, I. J.; Saven, J. G. Xe affinities of water-soluble cryptophanes and the role of confined water. *Chem. Sci.* **2015**, *6*, 7238−7248.

(22) Taratula, O.; Hill, P. A.; Khan, N. S.; Carroll, P. J.; Dmochowski, I. J. Crystallographic observation of 'induced fit' in a cryptophane host-guest model system. *Nat. Commun.* **2010**, *1*, 148.

(23) Mecozzi, S.; Rebek, J., Jr. The 55% solution: A formula for molecular recognition in the liquid state. *Chem. - Eur. J.* **1998**, *4*, 1016−1022.

(24) Spence, M. M.; Rubin, S. M.; Dimitrov, I. E.; Ruiz, E. J.; Wemmer, D. E.; Pines, A.; Yao, S. Q.; Tian, F.; Schultz, P. G. Functionalized xenon as a biosensor. *Proc. Natl. Acad. Sci. U. S. A.* **2001**, *98*, 10654−10657.

(25) Spence, M. M.; Ruiz, E. J.; Rubin, S. M.; Lowery, T. J.; Winssinger, N.; Schultz, P. G.; Wemmer, D. E.; Pines, A. Development of a functionalized xenon biosensor. *J. Am. Chem. Soc.* **2004**, *126*, 15287−15294.

(26) Wei, Q.; Seward, G. K.; Hill, P. A.; Patton, B.; Dimitrov, I. E.; Kuzma, N. N.; Dmochowski, I. J. Designing ^{129}Xe NMR biosensors for matrix metalloproteinase detection. *J. Am. Chem. Soc.* **2006**, *128*, 13274−13283.

(27) Roy, V.; Brotin, T.; Dutasta, J. P.; Charles, M. H.; Delair, T.; Mallet, F.; Huber, G.; Desvaux, H.; Boulard, Y.; Berthault, P. A cryptophane biosensor for the detection of specific nucleotide targets

DOI: 10.1021/acs.accounts.6b00309
Acc. Chem. Res. 2016, 49, 2179−2187

through xenon NMR spectroscopy. *ChemPhysChem* **2007**, *8*, 2082−2085.
(28) Kotera, N.; Dubost, E.; Milanole, G.; Doris, E.; Gravel, E.; Arhel, N.; Brotin, T.; Dutasta, J. P.; Cochrane, J.; Mari, E.; Boutin, C.; Leonce, E.; Berthault, P.; Rousseau, B. A doubly responsive probe for the detection of Cys4-tagged proteins. *J. Chem. Soc., Chem. Commun.* **2015**, *51*, 11482−11484.
(29) Seward, G. K.; Wei, Q.; Dmochowski, I. J. Peptide-mediated cellular uptake of cryptophane. *Bioconjugate Chem.* **2008**, *19*, 2129−2135.
(30) Seward, G. K.; Bai, Y.; Khan, N. S.; Dmochowski, I. J. Cell-compatible, integrin-targeted cryptophane-^{129}Xe NMR biosensors. *Chem. Sci.* **2011**, *2*, 1103−1110.
(31) Klippel, S.; Dopfert, J.; Jayapaul, J.; Kunth, M.; Rossella, F.; Schnurr, M.; Witte, C.; Freund, C.; Schröder, L. Cell tracking with caged xenon: Using cryptophanes as MRI reporters upon cellular internalization. *Angew. Chem., Int. Ed.* **2014**, *53*, 493−496.
(32) Palaniappan, K. K.; Ramirez, R. M.; Bajaj, V. S.; Wemmer, D. E.; Pines, A.; Francis, M. B. Molecular imaging of cancer cells using a bacteriophage-based ^{129}Xe NMR biosensor. *Angew. Chem., Int. Ed.* **2013**, *52*, 4849−4853.
(33) Boutin, C.; Stopin, A.; Lenda, F.; Brotin, T.; Dutasta, J.-P.; Jamin, N.; Sanson, A.; Boulard, Y.; Leteurtre, F.; Huber, G.; Bogaert-Buchmann, A.; Tassali, N.; Desvaux, H.; Carrière, M.; Berthault, P. Cell uptake of a biosensor detected by hyperpolarized ^{129}Xe NMR: The transferrin case. *Bioorg. Med. Chem.* **2011**, *19*, 4135−4143.
(34) Aaron, J. A.; Chambers, J. M.; Jude, K. M.; Di Costanzo, L.; Dmochowski, I. J.; Christianson, D. W. Structure of a (129)Xe-cryptophane biosensor complexed with human carbonic anhydrase II. *J. Am. Chem. Soc.* **2008**, *130*, 6942−6943.
(35) Chambers, J. M.; Hill, P. A.; Aaron, J. A.; Han, Z. H.; Christianson, D. W.; Kuzma, N. N.; Dmochowski, I. J. Cryptophane xenon-129 nuclear magnetic resonance biosensors targeting human carbonic anhydrase. *J. Am. Chem. Soc.* **2009**, *131*, 563−569.
(36) Taratula, O.; Bai, Y.; D'Antonio, E. L.; Dmochowski, I. J. Enantiopure cryptophane-^{129}Xe nuclear magnetic resonance biosensors targeting carbonic anhydrase. *Supramol. Chem.* **2015**, *27*, 65.
(37) Garcia, S.; Chavez, L.; Lowery, T. J.; Han, S. I.; Wemmer, D. E.; Pines, A. Sensitivity enhancement by exchange mediated magnetization transfer of the xenon biosensor signal. *J. Magn. Reson.* **2007**, *184*, 72−77.
(38) Schröder, L.; Lowery, T. J.; Hilty, C.; Wemmer, D. E.; Pines, A. Molecular imaging using a targeted magnetic resonance hyperpolarized biosensor. *Science* **2006**, *314*, 446−449.
(39) Bai, Y.; Hill, P. A.; Dmochowski, I. J. Utilizing a water-soluble cryptophane with fast xenon exchange rates for picomolar sensitivity NMR measurements. *Anal. Chem.* **2012**, *84*, 9935−9941.
(40) Ruppert, K.; Brookeman, J. R.; Hagspiel, K. D.; Mugler, J. P. Probing lung physiology with xenon polarization transfer contrast-(XTC). *Magn. Reson. Med.* **2000**, *44*, 349−357.
(41) Schlundt, A.; Kilian, W.; Beyermann, M.; Sticht, J.; Günther, S.; Höpner, S.; Falk, K.; Roetzschke, O.; Mitschang, L.; Freund, C. A xenon-129 biosensor for monitoring MHC-peptide interactions. *Angew. Chem., Int. Ed.* **2009**, *48*, 4142−4145.
(42) Schnurr, M.; Sydow, K.; Rose, H. M.; Dathe, M.; Schröder, L. Brain endothelial cell targeting via a peptide-functionalized liposomal carrier for xenon Hyper-CEST MRI. *Adv. Healthcare Mater.* **2015**, *4*, 40−45.
(43) Witte, C.; Martos, V.; Rose, H. M.; Reinke, S.; Klippel, S.; Schröder, L.; Hackenberger, C. P. R. Live-cell MRI with xenon Hyper-CEST biosensors targeted to metabolically labeled cell-surface glycans. *Angew. Chem., Int. Ed.* **2015**, *54*, 2806−2810.
(44) Rose, H. M.; Witte, C.; Rossella, F.; Klippel, S.; Freund, C.; Schröder, L. Development of an antibody-based, modular biosensor for ^{129}Xe NMR molecular imaging of cells at nanomolar concentrations. *Proc. Natl. Acad. Sci. U. S. A.* **2014**, *111*, 11697−11702.
(45) Riggle, B. A.; Wang, Y.; Dmochowski, I. J. A "smart" ^{129}Xe NMR biosensor for pH-dependent cell labeling. *J. Am. Chem. Soc.* **2015**, *137*, 5542−5548.
(46) Lowery, T. J.; Garcia, S.; Chavez, L.; Ruiz, E. J.; Wu, T.; Brotin, T.; Dutasta, J. P.; King, D. S.; Schultz, P. G.; Pines, A.; Wemmer, D. E. Optimization of xenon biosensors for detection of protein interactions. *ChemBioChem* **2006**, *7*, 65−73.
(47) Mynar, J. L.; Lowery, T. J.; Wemmer, D. E.; Pines, A.; Frechet, J. M. J. Xenon biosensor amplification via dendrimer-cage supramolecular constructs. *J. Am. Chem. Soc.* **2006**, *128*, 6334−6335.
(48) Meldrum, T.; Seim, K. L.; Bajaj, V. S.; Palaniappan, K. K.; Wu, W.; Francis, M. B.; Wemmer, D. E.; Pines, A. A xenon-based molecular sensor assembled on an MS2 viral capsid scaffold. *J. Am. Chem. Soc.* **2010**, *132*, 5936−5937.
(49) Stevens, T. K.; Palaniappan, K. K.; Ramirez, R. M.; Francis, M. B.; Wemmer, D. E.; Pines, A. HyperCEST detection of a ^{129}Xe-based contrast agent composed of cryptophane-A molecular cages on a bacteriophage scaffold. *Magn. Reson. Med.* **2013**, *69*, 1245−1252.
(50) Albert, M. S.; Schepkin, V. D.; Budinger, T. F. Measurement of Xe-129 T1 in blood to explore the feasibility of hyperpolarized Xe-129 MRI. *J. Comput. Assisted Tomogr.* **1995**, *19*, 975−978.
(51) Boutin, C.; Desvaux, H.; Carrière, M.; Leteurtre, F.; Jamin, N.; Boulard, Y.; Berthault, P. Hyperpolarized ^{129}Xe NMR signature of living biological cells. *NMR Biomed.* **2011**, *24*, 1264−1269.
(52) Bai, Y.; Wang, Y.; Goulian, M.; Driks, A.; Dmochowski, I. J. Bacterial spore detection and analysis using hyperpolarized ^{129}Xe chemical exchange saturation transfer (Hyper-CEST) NMR. *Chem. Sci.* **2014**, *5*, 3197−3203.
(53) Stevens, T. K.; Ramirez, R. M.; Pines, A. Nanoemulsion contrast agents with sub-picomolar sensitivity for xenon NMR. *J. Am. Chem. Soc.* **2013**, *135*, 9576−9579.
(54) Klippel, S.; Freund, C.; Schröder, L. Multichannel MRI labeling of mammalian cells by switchable nanocarriers for hyperpolarized xenon. *Nano Lett.* **2014**, *14*, 5721−5726.
(55) Wang, Y.; Dmochowski, I. J. Cucurbit[6]uril is an ultrasensitive Xe-129 NMR contrast agent. *J. Chem. Soc., Chem. Commun.* **2015**, *51*, 8982−8985.
(56) Wang, Y.; Roose, B. W.; Philbin, J. P.; Doman, J. L.; Dmochowski, I. J. Programming a molecular relay for ultrasensitive biodetection through ^{129}Xe NMR. *Angew. Chem., Int. Ed.* **2016**, *55*, 1733−1736.
(57) Kunth, M.; Witte, C.; Hennig, A.; Schröder, L. Identification, classification, and signal amplification capabilities of high-turnover gas binding hosts in ultra-sensitive NMR. *Chem. Sci.* **2015**, *6*, 6069−6075.
(58) Schnurr, M.; Sloniec-Myszk, J.; Dopfert, J.; Schröder, L.; Hennig, A. Supramolecular assays for mapping enzyme activity by displacement-triggered change in hyperpolarized Xe-129 magnetization transfer NMR spectroscopy. *Angew. Chem., Int. Ed.* **2015**, *54*, 13444−13447.
(59) Finbloom, J. A.; Slack, C. C.; Bruns, C. J.; Jeong, K.; Wemmer, D. E.; Pines, A.; Francis, M. B. Rotaxane-mediated suppression and activation of cucurbit[6]uril for molecular detection by ^{129}Xe hyperCEST NMR. *J. Chem. Soc., Chem. Commun.* **2016**, *52*, 3119−3122.
(60) Hane, F. T.; Smylie, P. S.; Li, T.; Ruberto, J.; Dowhos, K.; Ball, I.; Tomanek, B.; DeBoef, B.; Albert, M. S. HyperCEST detection of cucurbit[6]uril in whole blood using an ultrashort saturation pre-pulse train. *Contrast Media Mol. Imaging* **2016**, *11*, 285−290.
(61) Gilad, A. A.; Winnard, P. T.; van Zijl, P. C. M.; Bulte, J. W. M. Developing MR reporter genes: promises and pitfalls. *NMR Biomed.* **2007**, *20*, 275−290.
(62) Shapiro, M. G.; Ramirez, R. M.; Sperling, L. J.; Sun, G.; Sun, J.; Pines, A.; Schaffer, D. V.; Bajaj, V. S. Genetically encoded reporters for hyperpolarized xenon magnetic resonance imaging. *Nat. Chem.* **2014**, *6*, 629−634.
(63) Wang, Y.; Roose, B. W.; Palovcak, E. J.; Carnevale, V.; Dmochowski, I. J. A genetically encoded β-lactamase reporter for ultrasensitive ^{129}Xe NMR in mammalian cells. *Angew. Chem., Int. Ed.* **2016**, *55*, 8984−8987.
(64) Gilad, A. A.; McMahon, M. T.; Walczak, P.; Winnard, P. T.; Raman, V.; van Laarhoven, H. W. M.; Skoglund, C. M.; Bulte, J. W.

DOI: 10.1021/acs.accounts.6b00309
Acc. Chem. Res. 2016, 49, 2179−2187

M.; van Zijl, P. C. M. Artificial reporter gene providing MRI contrast based on proton exchange. *Nat. Biotechnol.* **2007**, *25*, 217−219.
(65) Kunth, M.; Witte, C.; Schröder, L. Continuous-wave saturation considerations for efficient xenon depolarization. *NMR Biomed.* **2015**, *28*, 601−606.
(66) Zaiss, M.; Schnurr, M.; Bachert, P. Analytical solution for the depolarization of hyperpolarized nuclei by chemical exchange saturation transfer between free and encapsulated xenon-(HyperCEST). *J. Chem. Phys.* **2012**, *136*, 144106.
(67) Martin, C. C.; Williams, R. F.; Gao, J. H.; Nickerson, L. D.; Xiong, J.; Fox, P. T. The pharmacokinetics of hyperpolarized xenon: implications for cerebral MRI. *J. Magn. Reson. Imaging* **1997**, *7*, 848−854.
(68) Ruppert, K. Biomedical imaging with hyperpolarized noble gases. *Rep. Prog. Phys.* **2014**, *77*, 116701.
(69) Lerouge, F.; Melnyk, O.; Durand, J. O.; Raehm, L.; Berthault, P.; Huber, G.; Desvaux, H.; Constantinesco, A.; Choquet, P.; Detour, J.; Smaihi, M. Towards thrombosis-targeted zeolite nanoparticles for laser-polarized Xe-129 MRI. *J. Mater. Chem.* **2009**, *19*, 379−386.
(70) Meldrum, T.; Bajaj, V. S.; Wemmer, D. E.; Pines, A. Band-selective chemical exchange saturation transfer imaging with hyperpolarized xenon-based molecular sensors. *J. Magn. Reson.* **2011**, *213*, 14−21.

DOI: 10.1021/acs.accounts.6b00309
Acc. Chem. Res. 2016, 49, 2179−2187